EM-based Model for RIS-aided Channel and its Achievable DoF

Nobhendu Chowdhury and Praful Mankar

***Abstract*—Reconfigurable intelligent surfaces (RISs) are emerging as a key technology under 6G paradigm, enabling programmable electromagnetic (EM) transformations for controlling wireless propagation. This paper develops a rigorous EM-based model for RIS-aided channels utilizing the wavenumber-spectrum representation of the Helmholtz equation. We formulate the RIS as a spatially varying reflection operator that multiplicatively modifies the incident field in space. Further, by applying a convex hull-based geometric interpretation of the convolution supports, we establish a Brunn–Minkowski-type bound on achievable DoF. Our analysis identifies unusable wavenumber as a primary degradation factor in non-isotropic environments. We propose a spectral centering operation at RIS to mitigate these losses and validate the model through simulations of multipath enrichment, which demonstrate that efficiency degrades with high transverse wavevectors.**

***Index Terms*—RIS channels, electromagnetic modeling, degrees of freedom, electromagnetic information theory.**

I. Introduction

Reconfigurable intelligent surfaces (RISs) represent an emerging technology that can manipulate electromagnetic (EM) waves to dynamically control the propagation environment and improve the performance and efficiency of sixth-generation (6G) wireless networks [1]. RISs are especially useful in challenging *non-isotropic scenarios* like urban areas or indoor environments which suffer from intense blockage effects [2]. RISs are expected to play a central role in enabling technologies such as stacked intelligent metasurfaces [3] and smart radio environments [4].

Conventional models for multiple-input multiple-output (MIMO) channels are typically based on geometric optics, spherical wave expansions, or simplified far-field assumptions [5]. These approximations often fail at high frequency or high-dimensional antenna arrays as expected in 6G to enable integrated sensing and communication (ISAC), holographic MIMO, etc. because they neglect high-resolution spatial correlations and evanescent components that dominate when the aperture is electromagnetically large or the sensing resolution requires sub-wavelength precision [6].

Emerging research in EM-based channel modeling has challenged these limitations by establishing EM information theory (EIT), which introduces an EM physical layer integrating Maxwell's equations with Shannon's communication theory [7]. It provides a formulation of mutual information and degrees of freedom (DoF) based on random EM fields [8]. These works greatly advocate for EM-consistent approaches over conventional discretized far-field MIMO models.

EM channel modeling: Traditional wireless channel models mostly rely on far-field plane-wave assumptions, which become inaccurate when antenna arrays operate in the near-field. On the other hand, Fourier spectral representations obtained by decomposing spherical waves into plane waves using Weyl's identity are accurate even in the near-field region [9]. Recent frameworks have further generalized reconfigurable EM environments by treating the RIS as a boundary condition within a continuous EM volume [10].

RIS path loss modeling: A path loss model for RIS-assisted links using the vector generalization of Green's theorem has been developed in [11], providing closed-form asymptotic expressions in near- and far-field regimes. The framework captured the effects of polarization, surface size, and array geometry.

Spatial sampling and DoF: An extension of the sampling theorem to three-dimensional EM fields was presented in [12], showing that fields are band-limited in wavenumber domain under arbitrary scattering conditions, and that such nature of band-limiting directly controls the number of independent DoF available in EM channels. Our work supplements these works by focusing specifically on the DoF scaling laws arising from spectral support expansion after interaction with RIS.

A. Contributions & Paper Outline

This paper derives an EM model for RIS placed in the propagation environment, as summarised below.

1) We present the RIS reflection coefficient in relation to the field desired at the receiver, which is an arbitrary target distribution designed for specific functionalities.
2) Next, we explore the role of the RIS in enhancing the DoF in non-isotropic scenarios. Specifically, we develop an upper bound on the additional realisable DoF.

The paper is organized as follows. In Section II, we look the foundational principles utilized in the investigations of the succeeding sections. In Section III, we provide a convolution-based model for the optimal RIS reflection coefficient for any arbitrary desired field in an isotropic propagation environment. In Section IV, we derive an upper bound for the DoF in an RIS-assisted EM channel from the convolution in Section III. In Section V, we present illustrative simulation results to validate the proposed ideas. A summary of this paper is presented in Section VI.

N. Chowdhury and P. Mankar are associated with Signal Processing and Communication Research Center (SPCRC) at International Institute of Information technology Hyderabad (IIIT-H), India. Email: nobhendu.chowdhury@research.iiit.ac.in and praful.mankar@iiit.ac.in.

B. Notations and Conventions

Bold letters indicate vectors and matrices. $\mathbb{R}^n$ denotes the n-dimensional Euclidean space of real numbers. We use upper (lower) case letters for wavenumber (spatial) quantities, e.g., $e(\mathbf{r})$ and $E(\mathbf{k})$ represent the electric field in the spatial and wavenumber domains respectively. Script letters are used to denote the spectral support of fields, e.g., $\mathscr{E} = \operatorname{supp} E$. The superscript ch stands for the convex hull of a set, e.g. $\mathscr{E}^{\mathrm{ch}}$ for $\mathscr{E}$. We write $\mathscr{E}_1 \subset \mathscr{E}_2$ to denote that $\mathscr{E}_1$ is a subset of $\mathscr{E}_2$, and $\mathscr{E}_1 \subsetneq \mathscr{E}_2$ to denote that it is a proper subset. $m(\cdot)$ denotes the Lebesgue measure.

II. Preliminaries

This section recalls the fundamental physical and mathematical principles underlying the spatial characterization of EM fields, which will be useful for studying DoF and information transfer in continuous-space EM propagation models.

A. Electromagnetic fields and the Helmholtz equation

Consider a monochromatic scalar electromagnetic field $e(\mathbf{r})$ transmitted from a source current density $j(\mathbf{r})$. The field propagates through a medium characterized by permittivity ϵ, permeability μ, and wave impedance $\eta = \sqrt{\mu/\epsilon}$. Under time-harmonic excitation with wavelength λ, the relationship between the source and the radiated field at arbitrary point $\mathbf{r}$ is governed by the *inhomogeneous Helmholtz equation* [13]:

$$\nabla^2 e(\mathbf{r}) + k^2 e(\mathbf{r}) = \mathrm{j}k\eta\, j(\mathbf{r}), \tag{1}$$

where $k = 2\pi/\lambda$ is the wavenumber. Eq. (1) describes a linear and space-invariant system in the spatial domain. Its impulse response is characterized by the scalar Green's function:

$$h(\mathbf{r}) = -\mathrm{j}k\eta\, G(\mathbf{r}), \quad \text{where} \quad G(\mathbf{r}) = \tfrac{e^{\mathrm{j}k\|\mathbf{r}\|}}{4\pi\|\mathbf{r}\|}. \tag{2}$$

For an arbitrary $j(\mathbf{r})$, the resulting field is expressed as:

$$e(\mathbf{r}) = \int_{\mathbb{R}^3} h(\mathbf{r}-\mathbf{s})\, j(\mathbf{s})\, d\mathbf{s}.$$

B. Plane-wave and Fourier representations

By applying the spatial Fourier transform to (1), we have:

$$E(\mathbf{k}) = H(\mathbf{k})\, J(\mathbf{k}), \tag{3}$$

where $E(\mathbf{k})$, $H(\mathbf{k})$, and $J(\mathbf{k})$ denote the wavenumber spectra of $e(\mathbf{r})$, $h(\mathbf{r})$, and $j(\mathbf{r})$, respectively. The wavenumber spectrum of $g(\mathbf{r})$ is: $G(\mathbf{k}) = \int_{\mathbb{R}^3} g(\mathbf{r}) e^{-\mathrm{j}\mathbf{k}\cdot\mathbf{r}} d\mathbf{r}$. The *wavenumber response* of the propagation medium follows directly from (2) as:

$$H(\mathbf{k}) = \frac{\mathrm{j}k\eta}{\|\mathbf{k}\|^2 - k^2}.$$

C. Propagating region and spatial bandwidth

In a homogeneous medium, we enforce the dispersion relation $\|\mathbf{k}\|^2 = k_x^2 + k_y^2 + k_z^2 = k^2$ and eliminate k_z to obtain the *angular spectrum representation*:

$$e(\mathbf{r}) = \frac{1}{(2\pi)^2} \int_{\mathbb{R}^2} E(k_x, k_y)\, e^{\mathrm{j}(k_x x + k_y y + k_z z)}\, dk_x\, dk_y, \tag{4}$$

where $E(k_x, k_y)$ is the spectrum on the plane $z = 0$, and

$$k_z(k_x, k_y) = \begin{cases} \sqrt{k^2 - (k_x^2 + k_y^2)}, & k_x^2 + k_y^2 \le k^2, \\ \mathrm{j}\sqrt{(k_x^2 + k_y^2) - k^2}, & \text{otherwise.} \end{cases} \tag{5}$$

Spectral components within the disk

$$\mathscr{D} = \{(k_x, k_y) \colon k_x^2 + k_y^2 \le k^2\} \tag{6}$$

correspond to *propagating* waves, while those outside $\mathscr{D}$ correspond to *evanescent* components that decay exponentially with z [14]. The multiplicative term $M(k_x, k_y; z) = e^{\mathrm{j}k_z(k_x,k_y)z}$ in (4), is the *migration factor*, and it describes how each spatial-frequency component at $z = 0$ evolves along z [12]. It determines the phase accumulation that each plane-wave component undergoes when migrating between two parallel planes separated by z:

$$E(k_x, k_y; z) = M(k_x, k_y; z)\, E(k_x, k_y). \tag{7}$$

This decomposition clarifies that free-space propagation acts as a low-pass filter in the spatial-frequency domain, with effective spatial bandwidth $m(\mathscr{D}) = \pi k^2 = \frac{4\pi^3}{\lambda^2}$.

D. Field degrees of freedom

The DoF of an EM field quantifies the number of independent spatial components that can be resolved within a finite region. Equivalently, DoF measures the dimensionality of the subspace spanned by the field with an orthogonal basis.

Each independent spectral component within $\mathscr{D}$, as defined in (6), corresponds to an orthogonal mode of the field, and thus contributes one DoF. However, the field may not occupy the full propagating disk $\mathscr{D}$, but rather a smaller spectral region $\mathscr{R} \subset \mathscr{D}$ determined by the scattering environment. In such cases, the spatial DoF is given by Landau's formula [15]:

$$\mathrm{dof} = \frac{m(A) m(\mathscr{R})}{(2\pi)^2}, \tag{8}$$

When $\mathscr{R} = \mathscr{D}$, one recovers the full bandwidth:

$$\mathrm{dof}_{\max} = \frac{m(A)\,\pi k^2}{(2\pi)^2} = \frac{m(A)}{4\pi}\left(\frac{2\pi}{\lambda}\right)^2 = \frac{\pi\, m(A)}{\lambda^2}. \tag{9}$$

III. EM Model for RIS

In this section, we present an expression for the reflection coefficient provided by the finite-size RIS with continuous surface $\mathcal{S}$ to obtain desirable properties of the received spectrum.

A. RIS reflection coefficient

As shown in Fig. 1, the RIS is assumed to be placed parallel to the $z = 0$ plane at distances z_T and z_R from the transmitter and receiver, respectively. The spectrum of field incident on the RIS is denoted by $E_{\mathrm{inc}}(k_x, k_y)$. Under the specific assumption of isotropic propagation, this can be written using (7) as:

$$E_{\mathrm{inc}}(k_x, k_y) = E_{\mathrm{T}}(k_x, k_y; z_T) = E_{\mathrm{T}}(k_x, k_y) e^{\mathrm{j}k_z(k_x,k_y)z_T},$$

where $E_{\mathrm{T}}(k_x, k_y)$ denotes the transmitted field. The passive RIS alters the phase profile of the incident field allowing us to implement general field transformations. The corresponding

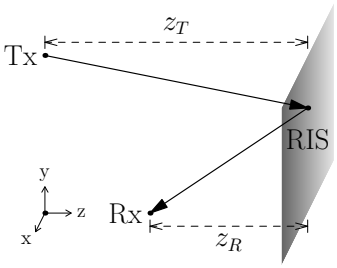

Fig. 1: Illustration of RIS Channel

reflection coefficient is denoted as $\xi(x,y) = e^{-\mathrm{j}\phi(x,y)}$ [4]. The fields incident on and reflected from the RIS, denoted as $e_{\mathrm{inc}}(x,y)$ and $e_{\mathrm{ref}}(x,y)$ respectively, follow the relation:

$$e_{\mathrm{ref}}(x,y) = \xi(x,y) e_{\mathrm{inc}}(x,y), \quad \text{for } (x,y) \in \mathcal{S} \tag{10}$$

Taking 2D Fourier transform on both sides gives:

$$\begin{aligned} E_{\mathrm{ref}}(k_x,k_y) &= \Xi(k_x,k_y) * E_{\mathrm{inc}}(k_x,k_y), \\ &= \int_{\mathbb{R}^2} \Xi(\kappa_x,\kappa_y) E_{\mathrm{inc}}(k_x-\kappa_x, k_y-\kappa_y) d\kappa_x d\kappa_y. \end{aligned} \tag{11}$$

For isotropic link between RIS and Rx, the received field is:

$$E_R(k_x,k_y) = E_{\mathrm{ref}}(k_x,k_y;z_R) = E_{\mathrm{ref}}(k_x,k_y) e^{\mathrm{j}k_z(k_x,k_y)z_R}.$$

Thus, using (11), we can write:

$$E_R(k_x,k_y) = e^{\mathrm{j}k_z(k_x,k_y)z_R} \big(\Xi(k_x,k_y) * E_{\mathrm{inc}}(k_x,k_y)\big).$$

Let $E_D(k_x,k_y)$ be the field desired at the receiver. We then require that $E_R(k_x,k_y) \approx E_D(k_x,k_y)$, which gives the required RIS reflection spectrum $\Xi^\star(k_x,k_y)$:

$$\Xi^\star(k_x,k_y) * E_{\mathrm{inc}}(k_x,k_y) \approx \tilde{E}_D(k_x,k_y), \tag{12}$$

where $\tilde{E}_D(k_x,k_y) := e^{-\mathrm{j}k_z(k_x,k_y)z_R} E_D(k_x,k_y)$.

B. Riemann-sum approximation

To numerically approximate the convolution in (12), we can use a *Riemann-sum discretization*. The wavenumber domain is sampled on a uniform rectangular grid of $N_x \times N_y$ points with spectral sampling intervals Δk_x and Δk_y. The sampling grid is spanned by points:

$$k_{p,q} = \left(k_x^{(p)}, k_y^{(q)}\right), \quad \text{for} \quad \begin{matrix} p = 0,\ldots,N_x-1, \\ q = 0,\ldots,N_y-1. \end{matrix}$$

Thus, (12) can be discretized as:

$$\sum_{u=0}^{N_x-1} \sum_{v=0}^{N_y-1} \Xi^\star[u,v] E_{\mathrm{inc}}[p-u, q-v]\ \Delta k_x \Delta k_y \approx \tilde{E}_D[p,q].$$

This can be expressed in the matrix form as:

$$\mathbf{C}\boldsymbol{\Xi}^\star \approx \tilde{\mathbf{E}}_{\mathbf{D}}, \tag{13}$$

where $\boldsymbol{\Xi}^\star$ and $\tilde{\mathbf{E}}_{\mathbf{D}}$ are the $N_x \times N_y$ matrix forms of $\Xi^\star[p,q]$ and $\tilde{E}_D[p,q]$ respectively, and $\mathbf{C}$ is the block convolution matrix whose (p,q)-th element is a matrix $\mathbf{C}_{(p,q)}$ written as:

$$\mathbf{C}_{(p,q)(u,v)} = E_{\mathrm{inc}}[p-u, q-v]\ \Delta k_x \Delta k_y.$$

Remark. *The problem of solving for $\boldsymbol{\Xi}^\star$ is non-convex since the passive RIS enforces $|\xi(x,y)| = 1$. With $\xi^\star(x,y) = \mathcal{F}^{-1}\{\Xi^\star(k_x,k_y)\}$, we have the optimization problem,*

$$\min_{\Xi} \|\mathbf{C}\boldsymbol{\Xi}^\star - \tilde{\mathbf{E}}_{\mathbf{D}}\|_2^2 \ \text{ s.t. } |\mathcal{F}^{-1}\{\boldsymbol{\Xi}^\star\}(x,y)| = 1\ \forall (x,y) \in \mathcal{S}.$$

This can be tackled in the style of Gerchberg-Saxton using Tikhonov regularization and alternate projection [16]. Beyond the modulus constraint, energy conservation implies a global inequality: the reflected field cannot exceed the available energy; i.e., $\iint_{\mathcal{S}} |e_{\mathrm{ref}}(x,y)|^2 dxdy \le \iint_{\mathcal{S}} |e_{\mathrm{inc}}(x,y)|^2 dxdy$. The desired field $E_D(x,y)$ must respect this constraint.

IV. DoF Formulation

This section presents a theoretical upper bound on the increment in the number of independent communication modes, i.e., additional DoF $\Delta\mathrm{dof}$, provided by the RIS-aided path relative to the direct Tx-Rx link.

A. Set-theoretic quantification

While the spatial and wavenumber domains are duals, the k-domain formulation is uniquely advantageous here, as it accounts for evanescent waves and near-field effects that conventional channel models fail to capture. Further, it transforms the complex interaction between the RIS and the incident field into a geometric convolution of their spectral supports, allowing us to derive fundamental dimensionality bounds that are not analytically tractable in the spatial domain.

In (11), denote the supports of the spectra of the reflected field, RIS coefficient and incident field as $\mathscr{S}_{\mathrm{ref}} = \mathrm{supp}\ E_{\mathrm{ref}}$, $\mathscr{S}_{\mathrm{RIS}} = \mathrm{supp}\ \Xi$ and $\mathscr{S}_{\mathrm{inc}} = \mathrm{supp}\ E_{\mathrm{inc}}$. The DoF offered by the field reflected from the RIS can be expressed using Landau's formula given in (8) as:

$$\mathrm{dof}_{\mathrm{ref}} = \frac{m(A)m(\mathscr{S}_{\mathrm{ref}})}{(2\pi)^2} \le \frac{m(A)m(\mathscr{S}_{\mathrm{RIS}} \oplus \mathscr{S}_{\mathrm{inc}})}{(2\pi)^2}, \tag{14}$$

where the inequality is obtained from the relation $\mathscr{S}_{\mathrm{ref}} \subset \mathscr{S}_{\mathrm{RIS}} \oplus \mathscr{S}_{\mathrm{inc}}$, which is obtained from the theory of convolution [17, Thm. 4.2.4]. Here, $\oplus$ denotes the Minkowski sum.

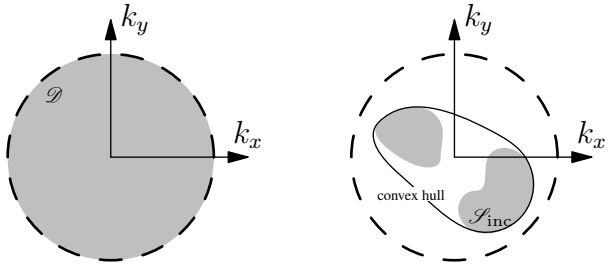

(a) isotropic (b) non-isotropic

Fig. 2: Blockage effects causing loss of support. $\mathscr{D}$ and $\mathscr{S}_{\mathrm{inc}}$ refer to propagating disk and incident field support respectively

In the case of arbitrary blockage creating a non-isotropic scattering environment, $\mathscr{S}_{\mathrm{inc}}$ does not occupy the entire propagating disk, i.e., $\mathscr{S}_{\mathrm{inc}} \subsetneq \mathscr{D}$, as shown in Fig. 2. Further, $\mathscr{S}_{\mathrm{inc}}$ would generally not be connected, which makes it difficult to directly calculate the field's bandwidth. Thus, to accurately

characterize the received DoF in (14), the embedding of $\mathscr{S}_{\text{inc}}$ with minimum measure is required [18]. Such an embedding, by definition, corresponds to the convex hull of $\mathscr{S}_{\text{inc}}$, denoted as $\mathscr{S}^{\text{ch}}_{\text{inc}}$. This gives the relation [17, Thm. 4.3.3]

$$\mathscr{S}^{\text{ch}}_{\text{ref}} = \mathscr{S}^{\text{ch}}_{\text{RIS}} \oplus \mathscr{S}^{\text{ch}}_{\text{inc}},$$

where $\mathscr{S}^{\text{ch}}_{\text{ref}}$, $\mathscr{S}^{\text{ch}}_{\text{RIS}}$ and $\mathscr{S}^{\text{ch}}_{\text{inc}}$ represent the convex hull of the respective supports of E_{ref}, Ξ and E_{inc}. Using this, (14) can be expressed as:

$$\text{dof}_{\text{ch}} = \frac{m(A)m(\mathscr{S}^{\text{ch}}_{\text{ref}})}{(2\pi)^2} = \frac{m(A)m(\mathscr{S}^{\text{ch}}_{\text{RIS}} \oplus \mathscr{S}^{\text{ch}}_{\text{inc}})}{(2\pi)^2}, \quad (15)$$

where dof_{ch} provides a fairly accurate estimate of dof_{ref}. We can lower bound (15) using Brunn-Minkowski inequality [19], i.e., $m(\mathscr{S}^{\text{ch}}_{\text{ref}})^{\frac{1}{2}} \geq m(\mathscr{S}^{\text{ch}}_{\text{inc}})^{\frac{1}{2}} + m(\mathscr{S}^{\text{ch}}_{\text{RIS}})^{\frac{1}{2}}$, as:

$$\text{dof}_{\text{ch}} \geq \frac{m(A)}{(2\pi)^2}\left[m(\mathscr{S}^{\text{ch}}_{\text{inc}}) + m(\mathscr{S}^{\text{ch}}_{\text{RIS}}) + 2\sqrt{m(\mathscr{S}^{\text{ch}}_{\text{inc}})m(\mathscr{S}^{\text{ch}}_{\text{RIS}})}\right] \quad (16)$$

The term $m(\mathscr{S}^{\text{ch}}_{\text{RIS}})$ in (16) suggests that the RIS offers additional DoF components to the reflected field. Further, the term $2\sqrt{m(\mathscr{S}^{\text{ch}}_{\text{inc}})m(\mathscr{S}^{\text{ch}}_{\text{RIS}})}$ suggests that the RIS does not merely add DoF; it non-linearly modifies the existing spatial support of the incident field.

B. The propagation constraint

Among the expanded spectral support offered upon reflection, only those components within the propagating disk $\mathscr{D}$, as defined in (6), correspond to propagating waves which ultimately carry information through space. To accommodate this behaviour, we introduce the propagation constraint:

$$\text{dof}_{\text{real}} = \frac{m(A)m(\mathscr{S}^{\text{ch}}_{\text{ref}} \cap \mathscr{D})}{(2\pi)^2} \leq \text{dof}_{\text{ch}}. \quad (17)$$

While (16) is a mathematical lower bound on the total available support, (17) defines a physical upper bound on the realisable DoF. Using the relation $\Delta\text{dof} = \text{dof}_{\text{real}} - \text{dof}_{\text{inc}}$, (16) and (17) yields the upper bound:

$$\Delta\text{dof} \leq \frac{m(A)}{(2\pi)^2}\left[m(\mathscr{S}^{\text{ch}}_{\text{RIS}}) + 2\sqrt{m(\mathscr{S}^{\text{ch}}_{\text{inc}})m(\mathscr{S}^{\text{ch}}_{\text{RIS}})}\right]. \quad (18)$$

As per (9), we also have a physical realisability constraint:

$$\text{dof}_{\text{max}} = \frac{\pi\, m(A)}{\lambda^2}.$$

Using the propagation constraint, we introduce a *spectral efficiency* factor η as:

$$\eta = \frac{\text{dof}_{\text{real}}}{\text{dof}_{\text{ref}}} \approx \frac{\text{dof}_{\text{real}}}{\text{dof}_{\text{ch}}} = \frac{m(\mathscr{S}^{\text{ch}}_{\text{ref}} \cap \mathscr{D})}{m(\mathscr{S}^{\text{ch}}_{\text{ref}})} \in (0, 1].$$

As the RIS generates additional spatial components, η eventually begins to drop, indicating that these components correspond to evanescent waves rather than usable DoF, causing *spectral spillover*, given by $m(\mathscr{S}^{\text{ch}}_{\text{ref}}) - m(\mathscr{S}^{\text{ch}}_{\text{ref}} \cap \mathscr{D})$.

C. The centering operation

Usually, the transmitted field is incident on the RIS at a non-zero angle of incidence θ_{inc}. This gives the incident field a mean wavevector of $\mathbf{k}_{\text{inc}} = k_{x_0}\hat{\mathbf{x}} + k_{y_0}\hat{\mathbf{y}}$. The incident field is accordingly expressed as:

$$e_{\text{inc}}(x, y) = e_{\text{T}}(x, y)\, e^{\text{j}(k_{x_0}x + k_{y_0}y)},$$

where $e_{\text{T}}(x, y)$ is the transmitted field acted upon by environmental scattering. Taking the Fourier transform, we get

$$E_{\text{inc}}(k_x, k_y) = E_{\text{T}}(k_x, k_y) * \delta(k_x - k_{x_0}, k_y - k_{y_0}),$$

which shifts the incident spectrum away from the center of the propagating disk (see Fig. 3(a)). Further, performing the RIS modifications on this shifted spectrum can lead to a higher extent of spectral spillover (highlighted in dark grey in Fig. 3(c)). To avoid this loss, the RIS can be designed to perform an initial centering operation to move the incident spectrum back towards the origin $(0, 0)$ before modifying the spectral components (see Fig. 3(b)). This ensures that the restored spectral components (and therefore, DoF) can actually propagate across the far-field (see Fig. 3(d)).

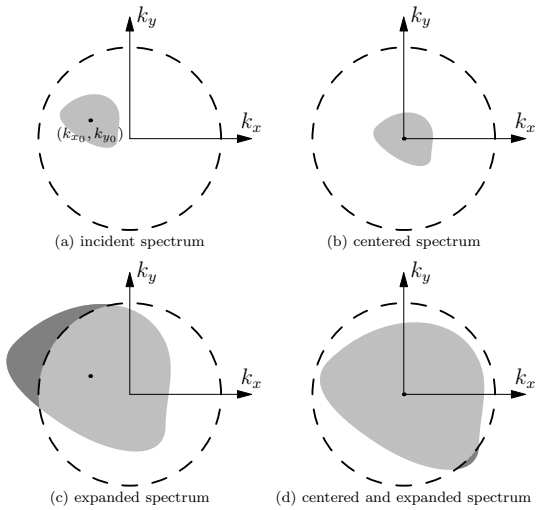

Fig. 3: Impact of centering of incident spectrum by RIS

For RIS reflection coefficient given by $\xi(x, y) = e^{-\text{j}\phi(x,y)}$, we can write:

$$\phi(x, y) = \underbrace{(k_{x_0}x + k_{y_0}y)}_{\text{centering term}} + \phi_{\text{diff}}(x, y), \quad (19)$$

where $\phi_{\text{diff}}(x, y)$ refers to the deterministic diffusion introduced by the RIS. Taking the example of multipath enrichment, where we might want to restore certain specific spectral components lost to scattering in the propagation environment, we choose $\Xi_{\text{diff}}(k_x, k_y) = \sum_{n=1}^{N} a_n \delta(k_x - k_{x_n}, k_y - k_{y_n})$, which translates to:

$$\phi_{\text{diff}}(x, y) = \arg\left(\sum_{n=1}^{N} a_n e^{-\text{j}(k_{x_n}x + k_{y_n}y)}\right), \quad (20)$$

where a_n is the strength of the n-th multipath component, and $\mathbf{k}_n = k_{x_n}\hat{\mathbf{x}} + k_{y_n}\hat{\mathbf{y}}$ is the n-th wavenumber vector.

V. Simulation & Discussion

We validate the proposed concept of spectral spillover using a multipath enrichment scenario having LoS incidence at angle θ_{inc} and N receivers placed at angles θ_n with respect to RIS. Each user receives a specific spectral component for direction θ_n. We evaluate spectral efficiency η against the normalised transverse incident wavenumber $\|\mathbf{k}_{\text{inc}}\|/k = \sin(\theta_{\text{inc}})$. To highlight the necessity of the centering operation, we take the diffusive phase $\phi_{\text{diff}}(x, y)$ to configure the RIS with and without centering, as given in (19) and (20).

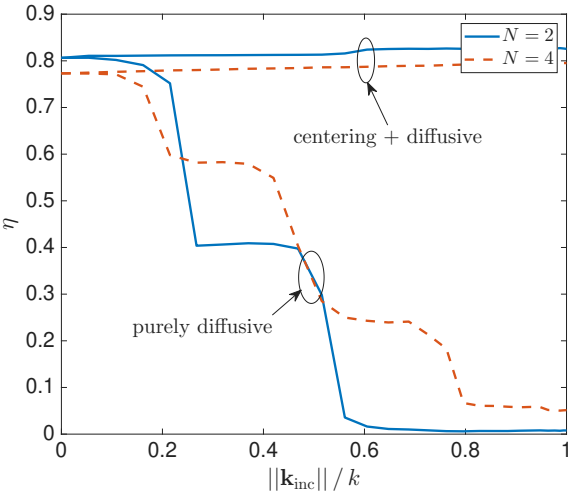

Fig. 4: Impact of spectral spillover on realizable DoF. For $N = 2$, $\theta_n = \{30^o, 60^o\}$, and for $N = 4$, $\theta_n = \{15^o, 30^o, 45^o, 60^o\}$.

Fig. 4 illustrates the behaviour of η for $N = 2$ and $N = 4$. In both cases, η remains high for near-normal incidence, i.e., $\|\mathbf{k}_{\text{inc}}\| \approx 0$. With centering, η remains high and stable irrespective of $\|\mathbf{k}_{\text{inc}}\|$. However, without centering, it exhibits a sharp multi-step degradation with increase in $\|\mathbf{k}_{\text{inc}}\|$. The discrete steps in the plots represent individual multipath components spilling into evanescent waves as $\|\mathbf{k}_{\text{inc}}\|$ increases, as illustrated in Fig. 3(c) for purely the diffusive case. A lower N allows for higher initial efficiency, while a higher N delays *total spillover* i.e., $\eta \approx 0$. Additionally, a higher N maintains a higher overall η even at high values of $\|\mathbf{k}_{\text{inc}}\|$. This is because a higher N offers a more distributed spectral support, which ensures that considerable spectral components lie within $\mathscr{D}$. These results empirically justify the centering operation in (19) to preserve DoF at high transverse wavenumber.

VI. Summary

This paper develops an EM model for RIS-aided communication systems using wavenumber-spectrum representation of the Helmholtz equation that captures the fundamental behaviour of the propagation of EM fields radiated by a source. In particular, the model utilizes the fields incident on and reflected from the RIS to characterize the reflection coefficient to generate a desirable field at the receiver. Further, using Landau's formulation for DoF, we use the above model to derive a Brunn-Minkowski-type bound on the additional DoF provided by the RIS. We also introduce the concept of spectral spillover and efficiency to motivate the necessity of a centering operation at the RIS.

References

[1] C. Huang, A. Zappone, G. C. Alexandropoulos, M. Debbah, and C. Yuen, "Reconfigurable intelligent surfaces for energy efficiency in wireless communication," *IEEE transactions on wireless communications*, vol. 18, no. 8, pp. 4157–4170, 2019.

[2] N. S. Perović, M. Di Renzo, and M. F. Flanagan, "Channel capacity optimization using reconfigurable intelligent surfaces in indoor mmwave environments," in *International Conference on Communications (ICC)*. IEEE, 2020, pp. 1–7.

[3] J. An, C. Xu, D. W. K. Ng, G. C. Alexandropoulos, C. Huang, C. Yuen, and L. Hanzo, "Stacked intelligent metasurfaces for efficient holographic MIMO communications in 6G," *IEEE Journal on Selected Areas in Communications*, vol. 41, no. 8, pp. 2380–2396, 2023.

[4] M. Di Renzo, A. Zappone, M. Debbah, M.-S. Alouini, C. Yuen, J. De Rosny, and S. Tretyakov, "Smart radio environments empowered by reconfigurable intelligent surfaces: How it works, state of research, and the road ahead," *IEEE journal on selected areas in communications*, vol. 38, no. 11, pp. 2450–2525, 2020.

[5] M. D. Migliore, "Horse (electromagnetics) is more important than horseman (information) for wireless transmission," *IEEE Transactions on Antennas and Propagation*, vol. 67, no. 4, pp. 2046–2055, 2018.

[6] C.-X. Wang, X. You, X. Gao, X. Zhu, Z. Li, C. Zhang, H. Wang, Y. Huang, Y. Chen, H. Haas *et al.*, "On the road to 6G: Visions, requirements, key technologies, and testbeds," *IEEE Communications Surveys & Tutorials*, vol. 25, no. 2, pp. 905–974, 2023.

[7] J. Zhu, Z. Wan, L. Dai, M. Debbah, and H. V. Poor, "Electromagnetic information theory: Fundamentals, modeling, applications, and open problems," *IEEE Wireless Communications*, vol. 31, no. 3, pp. 156–162, 2024.

[8] Z. Wan, J. Zhu, Z. Zhang, L. Dai, and C.-B. Chae, "Mutual information for electromagnetic information theory based on random fields," *IEEE Transactions on Communications*, vol. 71, no. 4, pp. 1982–1996, 2023.

[9] P. C. Clemmow, *The plane wave spectrum representation of electromagnetic fields: International series of monographs in electromagnetic waves*. Elsevier, 2013.

[10] D. Dardari, "Reconfigurable electromagnetic environments: A general framework," *IEEE Journal on Selected Areas in Communications*, vol. 42, no. 6, pp. 1479–1493, 2024.

[11] F. H. Danufane, M. Di Renzo, J. De Rosny, and S. Tretyakov, "On the path-loss of reconfigurable intelligent surfaces: An approach based on Green's theorem applied to vector fields," *IEEE Transactions on Communications*, vol. 69, no. 8, pp. 5573–5592, 2021.

[12] A. Pizzo, A. de Jesus Torres, L. Sanguinetti, and T. L. Marzetta, "Nyquist sampling and degrees of freedom of electromagnetic fields," *IEEE Transactions on Signal Processing*, vol. 70, pp. 3935–3947, 2022.

[13] A. Pizzo, L. Sanguinetti, and T. L. Marzetta, "Spatial characterization of electromagnetic random channels," *IEEE Open Journal of the Communications Society*, vol. 3, pp. 847–866, 2022.

[14] W. C. Chew, *Waves and fields in inhomogenous media*. John Wiley & Sons, 1999.

[15] M. Franceschetti, "On Landau's eigenvalue theorem and information cut-sets," *IEEE Transactions on Information Theory*, vol. 61, no. 9, pp. 5042–5051, 2015.

[16] R. Gerchberg and W. Saxton, "A practical algorithm for the determination of phase from image and diffraction plane pictures," *SPIE milestone series MS*, vol. 94, pp. 646–646, 1994.

[17] L. Hörmander, *The analysis of linear partial differential operators. 1: Distribution theory and Fourier analysis*, 2nd ed., ser. Classics in mathematics. Springer, 2003.

[18] D. P. Petersen and D. Middleton, "Sampling and reconstruction of wave-number-limited functions in N-dimensional Euclidean spaces," *Information and control*, vol. 5, no. 4, pp. 279–323, 1962.

[19] R. Osserman, "The isoperimetric inequality," *Bulletin of the American Mathematical Society*, vol. 84, no. 6, pp. 1182–1238, 1978.